Journal of Non-Crystalline Solids 533 (2020) 119898

Contents lists available at ScienceDirect

Journal of Non-Crystalline Solids

journal homepage: www.elsevier.com/locate/jnoncrysol

Highlighting the impact of shear strain on the SiO_2 glass structure: From experiments to atomistic simulations

C. Martinet[a,*], M. Heili[a], V. Martinez[a], G. Kermouche[b], G. Molnar[c], N. Shcheblanov[c,d], E. Barthel[e], A. Tanguy[c]

[a] Université de Lyon, Université Claude Bernard Lyon-1, UMR5306 CNRS, Institut Lumière Matière, 10 rue Ada Byron, F-69662, Villeurbanne, France
[b] Mines Saint-Etienne, Univ Lyon, CNRS UMR 5307LGF, Centre SMS, 158 Cours Fauriel, 42023 Saint-Etienne, France
[c] LaMCoS, INSA-Lyon, CNRS UMR5259, Université de Lyon, F-69621 Villeurbanne Cedex, France
[d] Université Paris-Est, Laboratoire NAVIER (UMR 8205), CNRS, ENPC, IFSTTAR, F-77420 Marne-la-Vallée, France
[e] Science and Engineering of Soft Matter, UPMC/CNRS/ESPCI PPMD UMR 7615, 10, rue Vauquelin,75231 Paris cedex 05, France

ARTICLE INFO

Keywords:
SiO_2 glass
Structure
Densification
Shear strain
Raman spectroscopy
High pressure

ABSTRACT

SiO_2 glass structure has been permanently modified by uniaxial compression. Within such a loading, the structure is supposed to be affected both by densification and shear flow. We propose to compare recovered silica samples with similar densities, initially deformed plastically under a hydrostatic compression or under a uniaxial compression. From micro-Raman spectroscopy experiments, the shear strain effects have been highlighted on the structural modifications of the glass and have been confirmed from molecular dynamic simulations. In particular, medium range order depends on the mechanical history in plastically deformed glasses. Indeed, both experiments and simulations demonstrate that small rings are favored when permanent shear strain acts with densification, thus allowing a structural signature identification of the densification process.

1. Introduction

Silicate glasses have been extensively studied to more understand the structure and its behavior under different extreme conditions, pressure [1,2,3], temperature [4,5]. Nevertheless, the links between structure and mechanical properties have not yet been clearly established. A better understanding of these links can give important technological perspectives for the improvement of the mechanical strength of silicate glasses. At the macroscopic scale, silicate glasses are brittle, nevertheless, plastic deformation occurs at the micron scale [6,7] or, for larger samples, under purely hydrostatic pressure [3,8,9]. Crack propagations get its start from plastic deformation at scales smaller than the microscopic scale. Then, a better understanding of this process will permit to improve mechanical resistance of glasses and decrease damages.

For pure silica, under hydrostatic conditions and room temperature, up to 9 GPa, silica behavior is effectively elastic [10,11]. Above 9 GPa, permanent structural changes occur and density progressively increases with the increase of the maximum pressure reached [12,13]. This onset pressure of hydrostatic plastic flow (or yield pressure) is known to decrease when shear stress is added to the compression [14]. Pure SiO_2 glass has a large ability to densify permanently, up to a density increase of 21% [12]. This mechanical behavior is considered as anomalous. On the contrary, many other glasses such as soda lime silicates or metallic glasses for example, are considered as normal glasses and exhibit mainly plastic shear flow, which is volume conserving (isochoric) [15,16]. This feature is known to play in a straight forward way on fracture patterns observed on indent cross-section [17].

Under micro-indentation, there is a distribution of strain states, with different combinations of densification and permanent shear. Complexity of the strain field induced by sharp indentation makes difficult the estimation of the shear stress applied, thus the effect of shear strain on Raman spectra cannot be observed directly. Micropillar compression is a good alternative, since its unconfined geometry and the expected strain and stress homogeneities allow getting large shear strain and a quite low densification [18,19].

Very recently, from molecular dynamic simulations, the impact of permanent shear strain on glass structure and how it affects Raman spectra has been highlighted for the first time [20]. Nevertheless, to the authors knowledge, no experimental study has been reported on the shear stress effects on the structure. In this paper, we propose to compare the structures between different amorphous silica samples plastically deformed by two different routes, hydrostatic compression/decompression in a diamond anvil cell and uniaxial compression of micro-

* Corresponding author.
E-mail address: christine.martinet@univ-lyon1.fr (C. Martinet).

https://doi.org/10.1016/j.jnoncrysol.2020.119898
Received 25 July 2019; Received in revised form 19 December 2019; Accepted 6 January 2020

pillars. The SiO_2 glass structure is composed of SiO_4 tetrahedral units connected together by oxygen atoms forming rings of different sizes, from 3 up to 10 units. The most probable size is six fold rings. This ring structure is a description of the medium range order. We have performed ex-situ micro-Raman spectroscopy experiments on recovered silica densified either after a hydrostatic compression with a diamond anvil cell or after a uniaxial compression on micro-pillars. In addition, atomic-scale simulations have been carried out [21]. Applying hydrostatic compression and shear at constant pressure, the silica samples were deformed and the ring statistic was analyzed as a function of permanent densification and compared to that resulting from other densification processes.

2. Methods

2.1. Experiments

The micro-pillars were fabricated using the same procedure detailed in Lacroix et al. [18], in which silica wafers were etched using reactive ion etching (RIE). The micro-pillars obtained are 4.0 μm in height and 4.8 μm in diameter, with a taper angle close to 6°. Individual silica pillars were axially compressed using a flat punch. More precisely, most of the pillars were deformed using a MTS-XP nanoindentation set-up as detailed in the work of Lacroix et al. [18]. However, this set-up being load-controlled, it was not possible to reach large plastic deformation in the pillars. Consequently, the in-situ Scanning Electron Microscope (SEM) Alemnis set-up was used to achieve larger plastic deformation as shown in the work of Kermouche et al. [19]. The main drawback of this set-up is the electron irradiation occurring during the compression. However, most experiments reporting modification of silica by electron irradiation were performed using a high electron beam energy (MeV and high dose) [22] and TEM microscopy [23], whose voltage and electron beam energy are significantly higher than the corresponding one used in a SEM. Moreover, Kermouche et al. [19] reported that beam-off experiments on the same pillars than those investigated in the present paper led to equivalent mechanical properties than those measured with beam-on experiments. It is thus expected that the electron beam of the used SEM would have a negligible impact on the silica structure.

Densified silica samples have been prepared from high hydrostatic pressure, above the elastic pressure limit i.e. 9 GPa at room temperature. For that, compression/decompression cycles have been carried out at different maximal pressures P_{max} using a diamond anvil cell (DAC) to prepare samples. P_{max} were chosen in order to obtain recovered silica glasses with similar densities to the densities measured on the compressed micro-pillar samples. Pieces of silica wafer used for the fabrication of the pillars were introduced in the DAC. In the experimental volume, a ruby chip is introduced in order to determine the pressure P_{max} from the R_1 luminescence line of Cr^{3+} [24,25]. The pressure transmitting medium was a mixture of methanol:ethanol:water (16:3:1), which has been reported to ensure hydrostaticity of the loading up to 15 GPa [26]. For DAC samples, micro-Raman spectra were performed using a Renishaw RM1000 spectrometer with excitation wavelength at 532 nm from a diode laser emission. For the compressed micro-pillars, Raman spectra were recorded with a Jobin-Yvon Aramis spectrometer. The incident light is emitted by a diode laser at 473 nm. A 100x objective (NA 0.95) has been used, the analysis volume corresponds to 3–4 μm in z and about 2 μm^2 in surface. The densification rate obtained after a plastic compression of micro-pillars is not homogeneous in z, and density is maximum close to the surface [19]. Then, the 473 nm laser has been focalized above the surface at +2 μm. For DAC compression, a long focal distance x50 objective has been used.

For DAC experiments, five different P_{max} have been chosen to get densified samples, with a densification ratio similar to those compressed micro-pillar samples. These P_{max} values were 9.8 GPa, 10.9 GPa, 12.1 GPa, 13 GPa and 13.8 GPa. All micro-Raman experiments have been performed ex-situ i.e. after uniaxial loading or hydrostatic compression, at atmospheric pressure.

Recovered densified silica samples obtained after uniaxial compression on micro-pillars or a hydrostatic compression cycle will be named Micro-pillar samples or DAC samples respectively.

2.2. Simulations

Silica samples were generated by sequential deposition of the atoms in a cubic simulation cell with a box length of 100 Å. The interaction between each particle was taken into account using the BKS potential [27] using the parameter setting of Yuan and Cormack [28]. The samples were heated then cooled to 0 K. The deformation was carried out by successively rescaling the atomic positions and applying a conjugated gradient energy minimization procedure. Details about the simulations are found in our recent papers [21,29].

Two kinds of deformations were applied: (i) hydrostatic compression and (ii) shear at zero pressure. In the hydrostatic case the axial size of the simulation box was reduced uniformly. The samples were sheared by tilting the simulation cell in one direction, while using a barostat to maintain zero axial stresses.

Every sample was deformed and then relaxed to the original stress state to obtain the desired densification state. After which the software I.S.A.A.C.S. [30] was used to calculate the smallest ring size distribution up to 9 Si atoms according to the method of Le Roux and Jund [31].

3. Results

Fig. 1 shows experimental Raman spectra of both non-densified silica and plastically deformed silica after an irreversible uniaxial compression of micro-pillar or after a hydrostatic compression. For the non-densified silica sample, the most intense band, named main band, shows a maximum intensity at around 433 cm^{-1}. This band corresponds to the bending mode of bridging oxygens ν_B (Si—O—Si) and its large half width is attributed to the distribution of the Si—O—Si angles [32,33]. The D_1, centered at 490 cm^{-1} and D_2, centered at 606 cm^{-1}, named the “defect” lines, are attributed to the breathing mode, corresponding to in-phase O-bending motion, of four fold and three fold rings respectively [34].

In order to determine the local densities of the recovered compressed micro-pillars and DAC samples, a calibration curve of the maximum of the main band as a function of the density has been

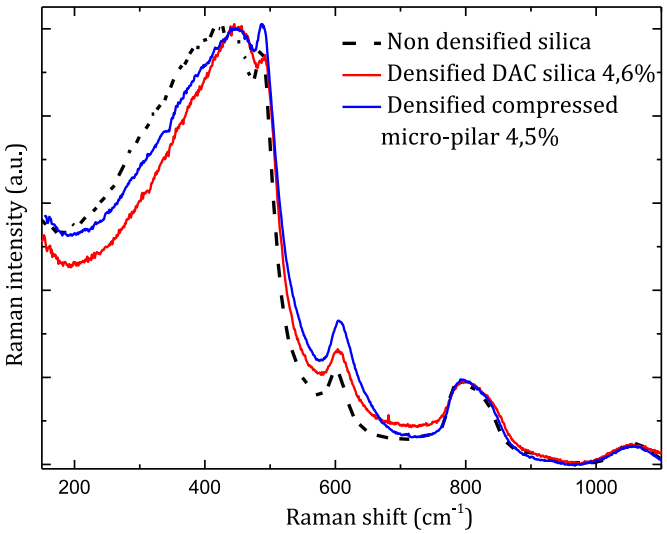

Fig. 1. Raman spectra of non-densified silica and 4.5% densified silica from hydrostatic and unaxial compressions.

established. This calibration curve is valid up to about 10% densification rate and does not depend on the densification process, i.e. whatever the pressure and temperature applied [35].

$$\nu_{MB} = 3.04\ (\pm 0.2)\frac{\Delta\rho}{\rho} + 433\ (\pm 2) \quad (1)$$

The densification rate is defined as:

$$\frac{\Delta\rho}{\rho} = \frac{\rho - \rho_0}{\rho}$$

where ρ and ρ_0 correspond respectively to density of the permanently densified silica and non-densified silica. Let us pay attention that densification after micro-compression is rather heterogeneous [19] contrary to classical uniaxial loadings. It is a consequence of pillars geometry and of the silica substrate. Therefore, the densification value derived from the calibration curve does not represent a homogeneous state of deformation. To avoid any misleading interpretations, we will refer to average densification in what follows.

Therefore, an "average densification" has been measured from the top of the surface of compressed micro-pillars up to 1–2 μm inside. These densification rate values have been deduced from Eq. (1), ranging from +1.5% to +8.1%, compared to non-densified silica. Different densified silica samples have been prepared at these different values of densities, either from a plastic uniaxial compression of micro-pillars or after a hydrostatic compression with different maximal pressure reached (P_{max}). It was thus possible to obtain similar densities from both methods, i.e. hydrostatic compression/decompression cycle and uniaxial compression. P_{max} is associated to a density for silica using calibration curve determined previously [12] and checked with the calibration curve, Eq. (1).

Figs. 1 and 2 exhibit Raman spectra of non-densified silica and permanent recovered densified silica obtained from hydrostatic compression cycle and from uniaxial compression for similar average densification rates of about 4.6% and about 8.0% respectively. After a plastic deformation, the main band shifts to higher frequencies and the D_2 band is more intense both for DAC and micro-pillar samples compared to non-densified silica. Nevertheless, for a similar density, Raman spectra exhibit large differences. In particular, the main band becomes narrower for DAC densified silica than for compressed micro-pillars. More precisely, to compare this evolution, a systematic determination of the half width at half maximum (HWHM) in the low frequency part, as a function of density has been deduced from the Raman spectra, see Fig. 3. Concerning the determination of the half width at half maximum

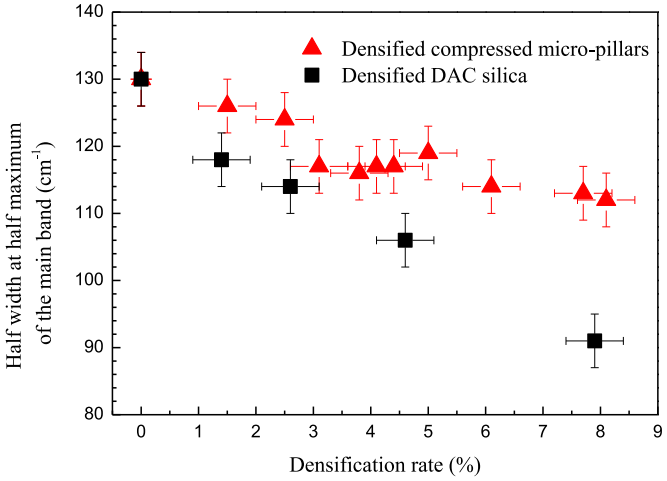

Fig. 3. Half width at half maximum of the main band as a function of average densification rate both for DAC and micro-pillar samples.

(HWHM), error bars are quite large (± 4 cm^{-1}) due to the band maximum intensity and the half width determinations. Moreover, concerning densification rate uncertainties, the main errors come from the calibration curve (1) and the determination of the main band frequency at maximum intensity which is about ± 0,5%. The HWHM depends strongly on silica density and on the compression method. Indeed, the non-hydrostatic compression induces a larger HWHM compared to the hydrostatic compression conditions. Nevertheless, the HWHM for compressed micro-pillars could be increased due to density gradient obtained after the compression. For that, further investigations should be necessary to establish the origin of the peak width. On Fig. 1, we observe that the D_1 band intensity remains unmodified in the case of DAC samples, whereas it increases after applying uniaxial compression. Concerning the D_2 band, a larger intensity has been observed for micro-pillar samples than for DAC samples. The D_2 band intensity has been systematically determined for all densified silica samples.

Fig. 4 demonstrates the evolution of the D_2 band area, normalized to the spectrum area from 200 cm^{-1} to 700 cm^{-1} as a function of density both for DAC and micro-pillar densified samples. The D_2 area normalized to the sum of the main band, the D_1 and the D_2 bands is linked to the 3-fold ring proportion because these three bands correspond to all the rings in the glass. The normalized D_2 band area uncertainties come mainly from the determination of the frequency of D_2 at maximum

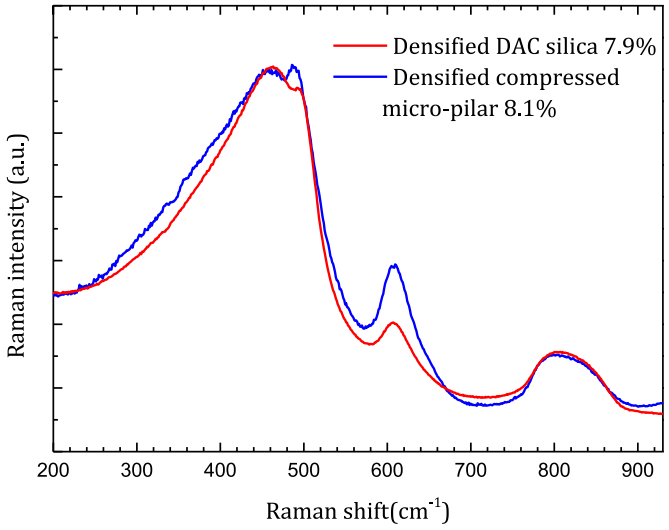

Fig. 2. Raman spectra of densified silica at 8% average densification rate both from hydrostatic and uniaxial compression.

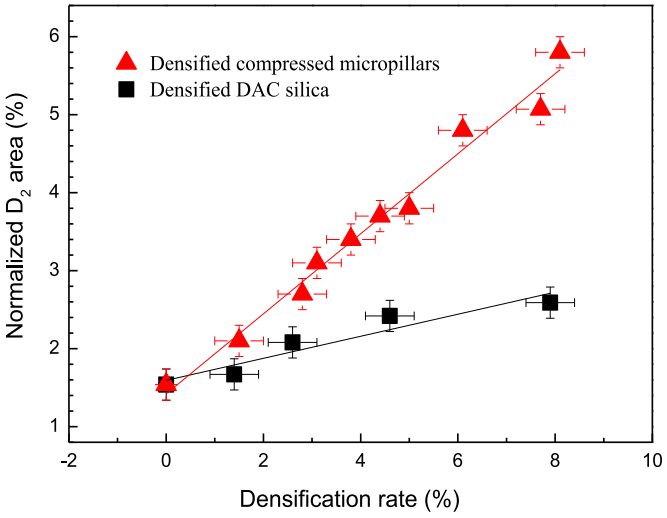

Fig. 4. Normalized D_2 area as a function of average densification rate both for DAC and micro-pillar samples.

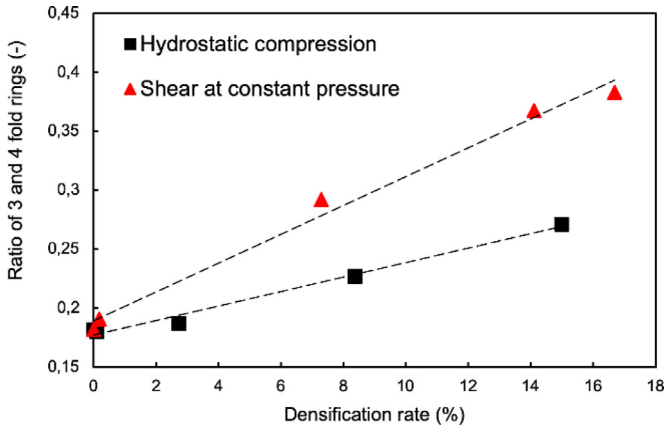

Fig. 5. Ratio of 3 to 4 fold rings as a function of permanent densification at zero stress from MD simulations.

intensity and the baseline determination: the error value has been estimated at about ± 0,2%. We observe that the normalized D_2 area increases linearly with density. Nevertheless, depending on compression conditions i.e. hydrostatic or not, the D_2 area increase is larger for uniaxial compression compared to hydrostatic one. The D_1 and D_2 bands exhibit a higher intensity for uniaxial micro-pillars silica in comparison to hydrostatic compression of silica for similar densities. Indeed, the normalized D_2 area evolves linearly as a function of densification rate and the slope is about 3.6 higher for uniaxial micro-pillars silica in comparison to hydrostatic compression samples (Fig. 4).

In parallel, we have calculated the evolution in the number of small rings by MD simulations. We find a marked increase in the total number of 3 fold rings upon shear at constant pressure, as compared to hydrostatic compression. In Fig. 5, the ratio of 3 to 4 fold rings is shown as a function of the permanent densification rate. It was shown already in the sixties, that plastification in silica is not volume preserving, and that densification occurs upon shear [14]. The increase in the relative number of 3 to 4 fold rings is more marked when the densification results from shear at constant pressure, than upon hydrostatic compression. The spectroscopic signature of 3 fold rings should thus be sensitive to the densification process.

4. Discussion

Permanent densification induces irreversible structural reorganization of glasses. High hydrostatic compression up to 9 GPa is fully elastic at room temperature for pure silica [3,10]. However, when temperature is simultaneously applied during a high pressure cycle or when shear stresses are introduced, elastic limit decreases [14,36]. Above the elastic limit, a permanent structural reorganization occurs with changes in the ring statistics and a decrease of the inter-tetrahedral Si—O—Si average angle [1,37,38]. The Si coordination also increases during the applied high pressure but is fully reversible for recovered sample [39,40].

On Fig. 1, the Raman spectra before and after a compression/decompression cycle show the evolution of the main band with a shift of the main band position (ω_{MB}) to higher frequencies and a decrease of its width. The maximum of the main band shifts to higher frequencies when densification increases both after an irreversible compression hydrostatic and not. The main band is usually related to the Si—O—Si angle distribution. From the central force model [32,33], inter-tetrahedral angles can be deduced:

$$\omega_{MB} = (2\alpha/m_o)^{(1/2)}(\cos\theta/2) \quad (2)$$

where ω_{MB} corresponds to the angular frequency of the Raman main band, α is the restoring central force constant between Si and O atoms, m_o is the oxygen atom mass (in bending vibration, Si atoms are fixed and O atoms move) and θ corresponds to the inter-tetrahedral angle.

Based on the values of literature, for non-densified silica glass, intertetrahedral angle averages vary from 136° to 151° depending on studies, from NMR, neutron diffraction measurements or molecular dynamics and ab-initio simulations. A good overview is available on the Tucker's paper [41]. In our paper, we choose an Si—O—Si angle average of 144° for normal silica glass. Starting from this value, we can deduce the relative variation of the intertetrahedral angles after plastic strain. An inter-tetrahedral angle of 144° corresponds to the average standard position of the main band centred at 433 cm^{-1} for non-densified silica [32]. Si—O bond length is almost unchanged after a permanent densification of SiO_2 glasses [33,42]. No Si coordination increase has been observed in permanently densified vitreous silica [43]. Then, the α force coefficient can be considered as constant for both non-densified and densified silica glasses. From Eq. (2), the ω_{MB} shift to higher frequencies is attributed to the decrease of the Si—O—Si angles. For example, at a densification rate of about 8%, the average angle should be about 141.7° both for DAC and micro-pillar samples.

The main band width is related to the Si—O—Si angle distribution. The HWHM of the main band is experimentally determined from the maximum of the main band position and from the low frequency part, because the high frequency part of the band contains the D_1 line, which evolves in intensity and in position as a function of density. The HWHM is about 130 cm^{-1} for the non-densified SiO_2 glass, indicating a large angles distribution. From Eq. (2), the Si—O—Si angle distribution obtained is 11°.

The HWHM main band decrease as a function of density is related to inter-tetrahedral angle distribution which is observed both for hydrostatic and uniaxial compression (Fig. 3). Nevertheless, this decrease is lower for the micro-pillar samples than for the DAC samples. For example, concerning the densified samples with a 8% densification rate, the HWHM is about 90 cm^{-1} after hydrostatic compression and it is about 112 cm^{-1} after uniaxial compression. From these above values and Eq. (2), the corresponding Si—O—Si angle distributions are 7.7 ± 0.7° for DAC sample and 9.5 ± 0.7° for micro-pillar sample. Uncertainties in the calculation of Si—O—Si angle distributions is mainly due to error on the determination of the HWHM of the main band. After plastic compression, the structure has been permanently reorganized and corresponds to a more homogeneous glass in terms of inter-tetrahedral angle distribution, particularly after a hydrostatic compression. Nevertheless, after uniaxial compression, the disorder in terms of Si—O—Si angle distribution remains apparently higher. The HWHM increase could be induced by gradient densification in the micropillar after the uniaxial compression. Very recently, Raman spectra of SiO_2 glasses have been theoretically determined before and after a plastic shear flow [20]. In this paper, the authors pointed out that the Si—O—Si distribution does not change much after a plastic shear flow compared to non-densified silica, whereas this distribution clearly decreases with a hydrostatic compression from MD simulation [8]. Then, our results confirm experimentally these theoretical studies and show that the silica glass has a more homogeneous structure after an irreversible hydrostatic compression than after applying shear stress, in terms of Si—O—Si angle distribution.

Molecular dynamics simulations on silica glass demonstrated that a permanent anisotropy has been created under shear flow on silica glass [44]. This result has been recently confirmed experimentally by X-ray diffraction experiments [45]. In particular, Sato et al. have put in evidence that shear stresses have an impact on the structure at intermediate range order, observing the change in the first sharp diffraction peak with shear stress.

Nevertheless, the densification pattern reveals a large density gradient demonstrated from finite element modeling [19] and this theoretical result could also explain the large Si—O—Si distribution. Indeed, the measured volume in our present micro-Raman experiments is larger than the density variation on the compressed micro-pillars. It is why caution has to be taken when comparing average densification

measured on the top of micro-pillar and the one measured after hydrostatic compression.

The normalized D_1 and D_2 lines area can be directly connected to the evolution of the relative population of four and three fold rings in the silica [34], recently confirmed by small scale Molecular Simulation [46]. Ring statistics in densified SiO_2 glass have been described both by theoretical and experimental studies. Results on recovered densified samples from cold hydrostatic compression show an increase of the small rings and a decrease of large rings [8,35,47]. When temperature is applied during the compression, the ring statistic doesn't evolve significantly [43]. In our present study, D_2 area increases whatever the applied compression conditions when silica density increases (Fig. 4). Nevertheless, the D_2 area increase is significantly more pronounced after a strongly non-hydrostatic pressure, i.e. after uniaxial compression of the micro-pillar samples, compared to a hydrostatic compression. For example, for a densification rate of about 8%, the D_2 line area is more than twice larger for the micro-pillar samples than for DAC samples. This indicates that shear deformation facilitates the formation of three fold rings at the expense of larger ring sizes. Our present experimental result is confirmed from our present simulation study (Fig. 5). Indeed, we put in evidence that shear strain has a significant impact on the structure at the middle range order of plastically deformed silica glass, with a significant increase of 3 fold rings upon shear.

Our experimental and numerical results thus confirm the role of the different preparation protocols, and of the different loading paths on the reorganization of the structure and its spectroscopic signatures. In particular, we show a significant increase of the 3 fold ring proportion at the expense of larger rings, under hydrostatic compression and more markedly under shear at constant pressure. A similar increase has been also put in evidence from simulations of the densification process under laser irradiation [48].

5. Conclusion

An original study of the influence of shear strain on the structure of densified silica glasses has been performed both experimentally and with molecular dynamics simulations. Concerning the experimental study, micro-pillars have been uniaxially compressed above the elastic limit. Due to their geometry, they exhibit a large shear strain. To highlight the impact of shear strain on the structure, for the first time, we have compared the recovered micro-pillars with recovered silica samples from hydrostatic irreversible compression. The silica glass samples structure has been analyzed with ex-situ Raman spectroscopy. This experimental study of densified silica glasses has been compared with numerical simulations. Both studies point out that the creation of 3 fold rings is favored by shear stresses at the expense to larger rings. Indeed, the relative proportion of 3 fold rings increases both for hydrostatic cold compression and uniaxial compression, as was shown already in the case of laser induced densification [48-49]. This increase is linear as a function of the resulting density. Nevertheless, after a plastic shear strain, for similar densities, the 3-fold rings proportion is significantly higher than for hydrostatic compression, thus affecting the amplitude of the D_2 band in the Raman spectra as a signature of the specificities of the related stress tensor.

Authors contribution

C. Martinet, M. Heili, V. Martinez carried out the DAC experiments and performed all the Raman measurements and data analysis. G. Kermouche and E. Barthel carried out the micro-pillar compression experiments. G. Molnar, N. Shcheblanov and A. Tanguy performed the atomistic simulations. All authors contributed to the interpretation of the data. C. Martinet wrote the paper, with the help of all the other authors.

Declaration of Competing Interest

The authors declare that they have no known competing financial interests or personal relationships that could have appeared to influence the work reported in this paper.

Acknowledgments

The authors would like to thank the spectrometry center CECOMO at University Lyon 1-France (CECOMO) for the using of Raman spectrometers. The present work was supported by ANR. MECASIL and by ANR MULTISIL, French program facility.

References

[1] C.H. Polsky, K.H. Smith, G.H. Wolf, J. Non-Cryst. Solids 248 (1999) 159–168.
[2] K. Trachenko, M.T. Dove, J. Phys. : Condens. Matter 14 (2002) 7449–7459.
[3] B. Champagnon, C. Martinet, M. Boudeulle, D. Vouagner, C. Coussa, T. Deschamps, L. Grosvalet, J. Non-Cryst. Solids 354 (2008) 569–573.
[4] A.E. Geissberger, F.L. Galeener, Phys. Rev. B 28 (1983) 3266.
[5] C. Martinet, V. Martinez, C. Coussa, B. Champagnon, M. Tomozawa, J. Appl. Phys. 103 (2008) 083506.
[6] A. Perriot, D. Vandembroucq, E. Barthel, V. Martinez, L. Grosvalet, Ch. Martinet, B. Champagnon, J. Am. Ceram. Soc. 89 (2006) 596–601.
[7] G.K. Aakermann, K. Januchta, J.A.L. Pedersen, M.N. Svenson, S.J. Rzoska, J. Non-Cryst. Solids 426 (2015) 175–183.
[8] L. Huang, J. Kieffer, Phys. Rev. B 69 (2004) 224204.
[9] R.J. Hemley, H.K. Mao, P.M. Bell, B.O. Mysen, Phys. Rev. Lett 57 (1986) 747.
[10] P.W. Bridgman, I. Simon, J. Appl. Phys. 24 (1953) 405–413.
[11] G.E. Walrafen, P.N. Krishnan, J. Chem. Phys. 74 (1981) 5328–5330.
[12] T. Rouxel, H. Ji, T. Hammouda, A. Moréac, Phys. Rev. Lett. 100 (2008) 225501.
[13] A. Polian, M. Grimsditch, Phys. Rev. B 47 (1993) 13979.
[14] J.D. Mackenzie, J. Am. Ceram. Soc 46 (1963) 461–470.
[15] G. Kermouche, E. Barthel, D. Vandembroucq, Ph. Dubujet, Acta Mater. 56 (2008) 3222–3228.
[16] A. Kassir-Bodon, T. Deschamps, C. Martinet, B. Champagnon, J. Teisseire, G. Kermouche, Int. J. Appl. Glass Sci. 3 (2012) 29–35.
[17] A. Arora, D.B. Marshall, B.R. Lawn, M.V. Swain, J. Non-Cryst. Solids 31 (1979) 415–428.
[18] R. Lacroix, G. Kermouche, J. Teisseire, E. Barthel, Acta Mater. 60 (2012) 5555–5566.
[19] G. Kermouche, G. Guillonneau, J. Michler, J. Teisseire, E. B.arthel, Perfectly plastic flow of silica glass, Acta Mater 114 (2016) 146–153.
[20] N.S. Shcheblanov, B. Mantisi, P. Umari, A. Tanguy, J. Non-Cryst. Solids 428 (2015) 6–19.
[21] G. Molnar, P. Ganster, A. Tanguy, E. Barthel, G. Kermouche, Acta Mater. 111 (2016) 129–137.
[22] N. Ollier, K. Piven, C. Martinet, T. Billotte, V. Martinez, D. Neuville, M. Lancry, J. Non-Cryst. Solids 476 (2017) 81–86.
[23] M. Mackovic, F. Niekiel, L. Wondraczek, E. Spiecker, Acta Mater. 79 (2014) 363–373.
[24] G.J. Piermarini, S. Block, J.D. Barnett, R.A. Forman, J. Appl. Phys. 46 (1975) 2774–2780.
[25] H.K. Mao, J. Xu, P.M. Bell, J. Geophys. Res. B 91 (1986) 4673.
[26] S. Klotz, J.-.C. Chervin, P. Munsch, G. Le Marchand, J. Phys. D 42 (2009) 075413.
[27] B.W.H. van Beest, G.J. Kramer, R.A. van Santen, Phys. Rev. Lett. 64 (1990) 1955.
[28] X. Yuan, A.N. Cormack, J. Non-Cryst. Solids 283 (2001) 69–87.
[29] G. Molnár, P. Ganster, A. Tanguy, Phys. Rev. E 95 (2017) 043001.
[30] S. Le Roux, V. Petkov, J. Appl. Cryst. 43 (2010) 181–185.
[31] S. Le Roux, P. Jund, Comput. Mater. Sci. 49 (2010) 70–83.
[32] P.N. Sen, M.F. Thorpe, Phys. Rev. B 15 (1977) 4030.
[33] B. Hehlen, J. Phys. Cond. Mat. 22 (2012) 025401.
[34] P. Umari, X. Gonze, A. Pasquarello, Phys. Rev. lett. 90 (2003) 027401.
[35] C. Martinet, A. Kassir-Bodon, T. Deschamps, A. Cornet, S. Le Floch, V. Martinez, B. Champagnon, J. Phys. Condens. Matter 27 (2015) 325401.
[36] P. McMillan, B. Piriou, R. Couty, J. Chem. Phys. 81 (1984) 4234.
[37] L. Davila, M. Caturla, A. Kubota, B. Sadigh, T. Dıaz de la Rubia, J.F. Shackelford, S.H. Risbud, S.H. Garofalini, Phys. Rev. Lett. 91 (2003) 205501.
[38] H. Sugiura, T. Yamadaya, J. Non-Cryst. Solids 144 (1992) 151–158.
[39] C. Meade, R.J. Hemley, H.K. Mao, Phys. Rev. Lett. 69 (1992) 1387.
[40] C.J. Benmore, E. Soignard, S.A. Amin, M. Guthrie, S.D. Shastri, P.L. Lee, J.L. Yarger, Phys. Rev. B 81 (2010) 054105.
[41] M.G. Tucker, D.A. Keen, M.T. Dove, K. Trachenko, J. Phys. Condens. Matter 17 (2005) S67.
[42] Y. Shimada, M. Okuno, Y. Syono, M. Kikuchi, K. Fukuoka, N. Ishizawa, Phys. Chem. Min. 29 (2002) 233–239.
[43] B. Poe, C. Romano, G. Henderson, J. Non-Cryst. Solids 341 (2004) 162–169.
[44] C.L. Rountree, D. Vandembroucq, M. Talamali, E. Bouchaud, S. Roux, Phys. Rev. Lett. 102 (2009) 19550.
[45] T. Sato, N. Funamori, T. Yagi, J. Appl. Phys. 114 (2013) 103509.
[46] P. Umari, X. Gonze, A. Pasquarello, Phys. Rev. Lett. 90 (2003) 027401.
[47] J. Burgin, C. Guillon, P. Langot, F. Vallée, B. Hehlen, M. Foret, Phys. Rev. B 78 (2008) 184203.
[48] N.S. Shcheblanov, M.E. Povarnitsyn, K.N. Mishchik, A. Tanguy, Phys. Rev. B 97 (2018) 054106.
[49] N.S. Shcheblanov, M.E. Povarnitsyn, Europhys. Lett. 114 (2016) 26004.